



Challenges posed by high-resolution spectropolarimetric observations of pulsating stars

**S. Hubrig, S. Järvinen, T. A. Carroll, I. Ilyin
(Leibniz-Institut für Astrophysik, Potsdam),
M. Schöller (ESO), M. Briquet (Ulg, Liege), et al.**



Pulsating stars on the upper main sequence

- Due to the strong and rapid changes of line profile position and profile shape in the spectra of pulsating stars, high-resolution spectropolarimetric observations frequently fail to show credible magnetic field measurements.
- We discuss our recent attempts to take into account the impact of pulsations for the field measurements.

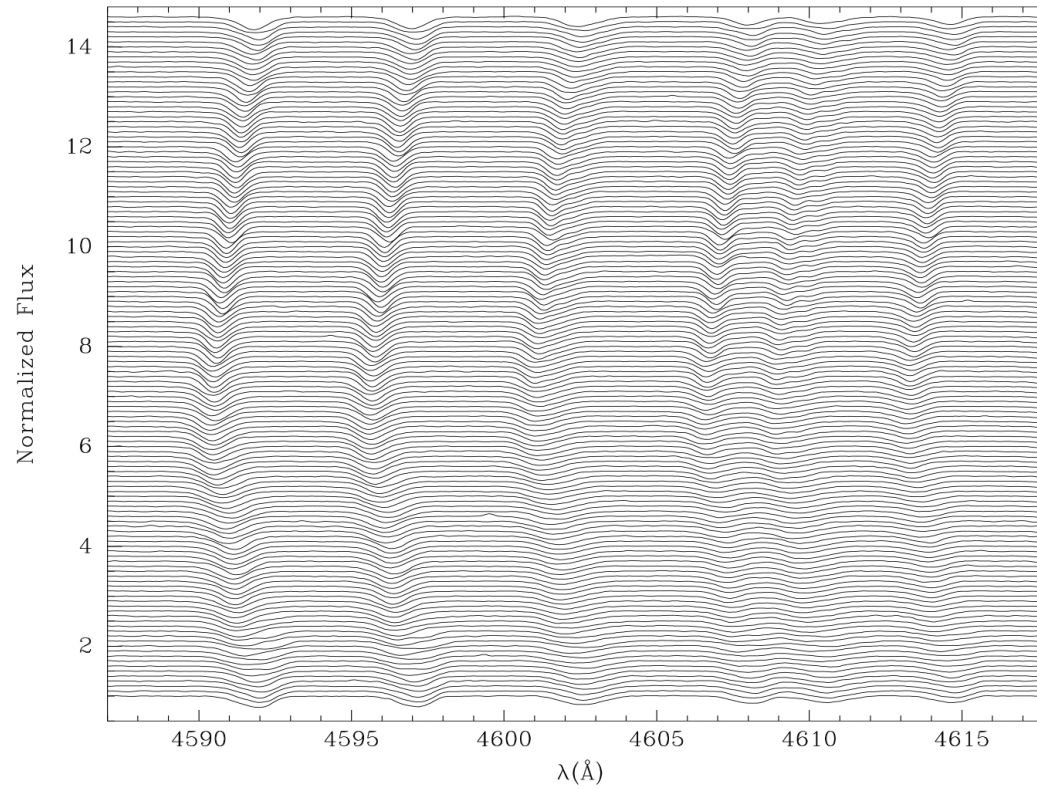
B-type stars

Depending on their spectral and photometric behavior, the main-sequence B-type stars are assigned to different groups:

- β Cephei stars
- slowly pulsating B (SPB) stars,
- He-rich and He-deficient Bp stars,
- Be stars,
- BpSi stars,
- HgMn stars
- normal B-type stars.

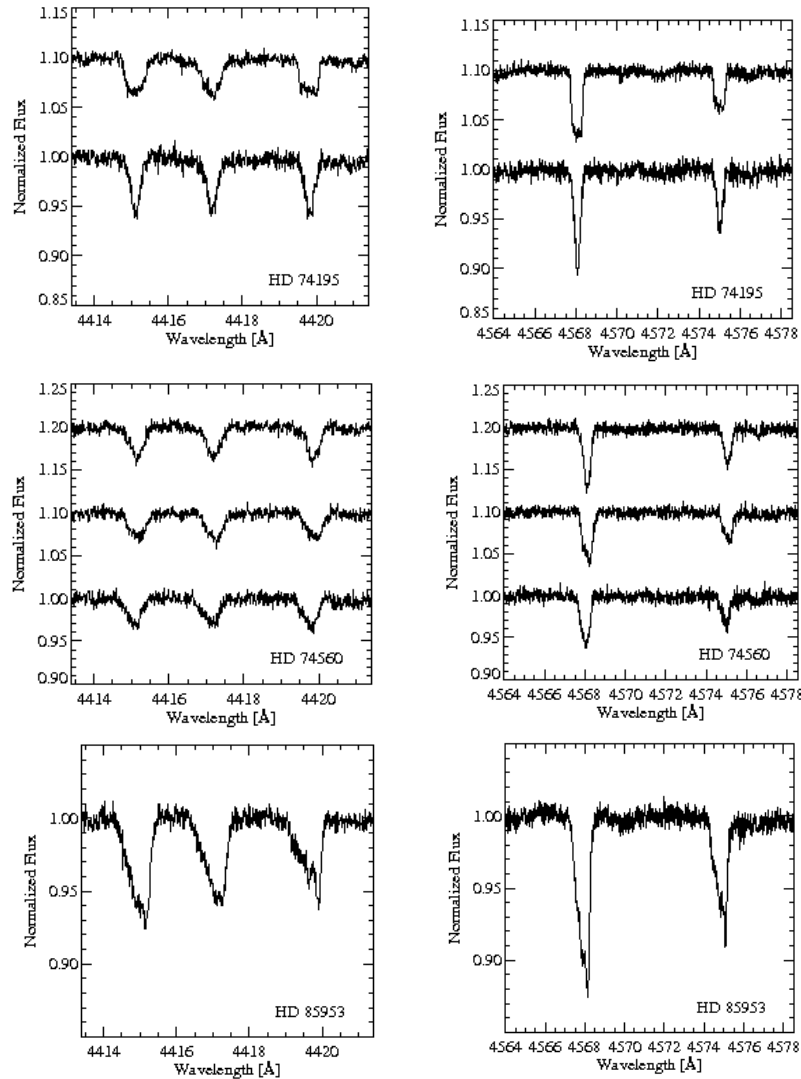
These groups are characterized by different magnetic field geometry and strength, from fields below the detection limit of a few Gauss up to tens of kG.

Line profile variability for the β Cephei pulsator V1449 Aql (Hubrig et al. 2011)



FEROS time series; Radial mode of frequency of 5.487 d^{-1}

Spectral variability evident in HARPS spectra of SPB stars (Hubrig et al. 2013)



From top to bottom:
strongly asymmetric and variable
line profiles in HARPS Stokes I
spectra of HD 74195, HD 74560,
and HD 85953.

Two O II lines and one Fe III line in
the region 4414-4420 Å (left),
Si III lines in the region 4566-4576 Å
(right).

Magnetic field observations of pulsating stars and inconsistencies in the interpretation of the field measurements

Silvester et al. (2008) reported that their observations indicate that magnetic β Cephei and SPB stars are rather rare.

But see Alecian et al. (2014): Out of the discovered 9 magnetic early B-type stars, 6 targets were suggested to exhibit pulsations.

Magnetic fields are not common in pulsating stars (Silvester et al. 2008)

in one star (16 Peg), but find no evidence of the presence of fields in the remaining 11. In the β Cep stars, we detect a field in ξ^1 CMa, but not in any of the remaining seven stars. Finally, neither of the two B-type emission-line stars shows any evidence of magnetic field. Based on our results, we conclude that fields are not common in SPB, β Cep and B-type emission-line stars, consistent with the general rarity of fields in the broader population of main sequence B-type stars. A relatively small, systematic underestimation of the error bars associated with the UV Focal Reducer and Low Dispersion Spectrograph for the Very Large Telescope (FORs1) longitudinal field measurements of Hubrig et al. could in large part explain the discrepancy between their results and those presented here.

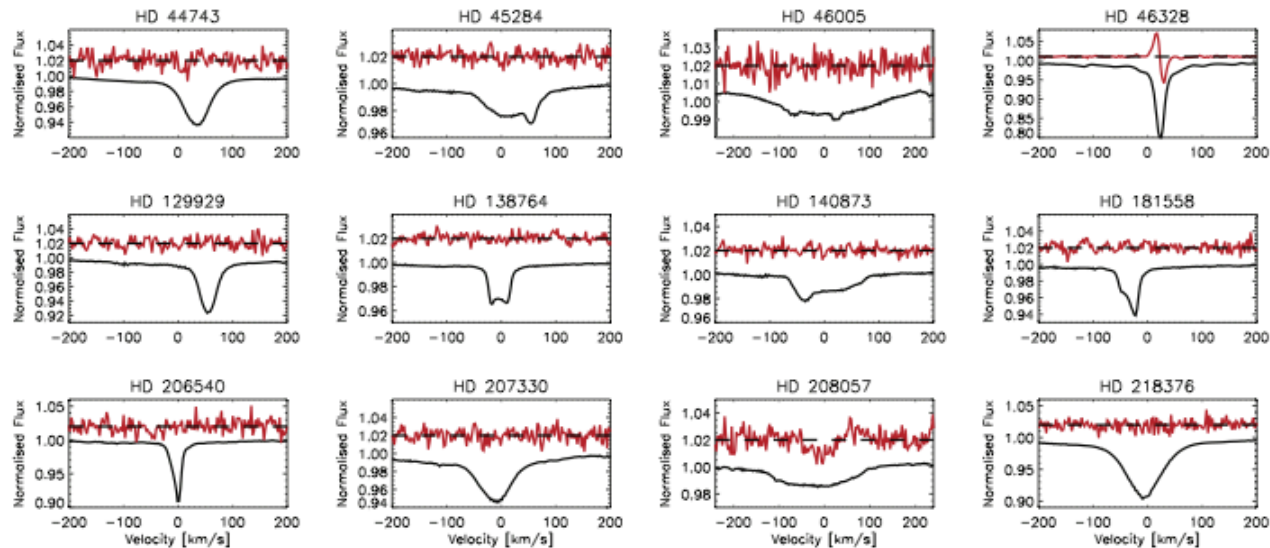


Figure 2. Least-squares deconvolved profiles of the SPB and β Cep stars (for stars with multiple observations, a single example is shown). Each panel represents a different star, with the bottom curve showing the LSD mean intensity (Stokes I) profile and the top curve showing the circular polarization Stokes V profile. Note the frequently asymmetric or otherwise distorted profile shapes due to pulsation and binarity.

Out of the discovered 9 magnetic early B-type stars, 6 targets are suggested to exhibit pulsations (Alecian et al. 2014)

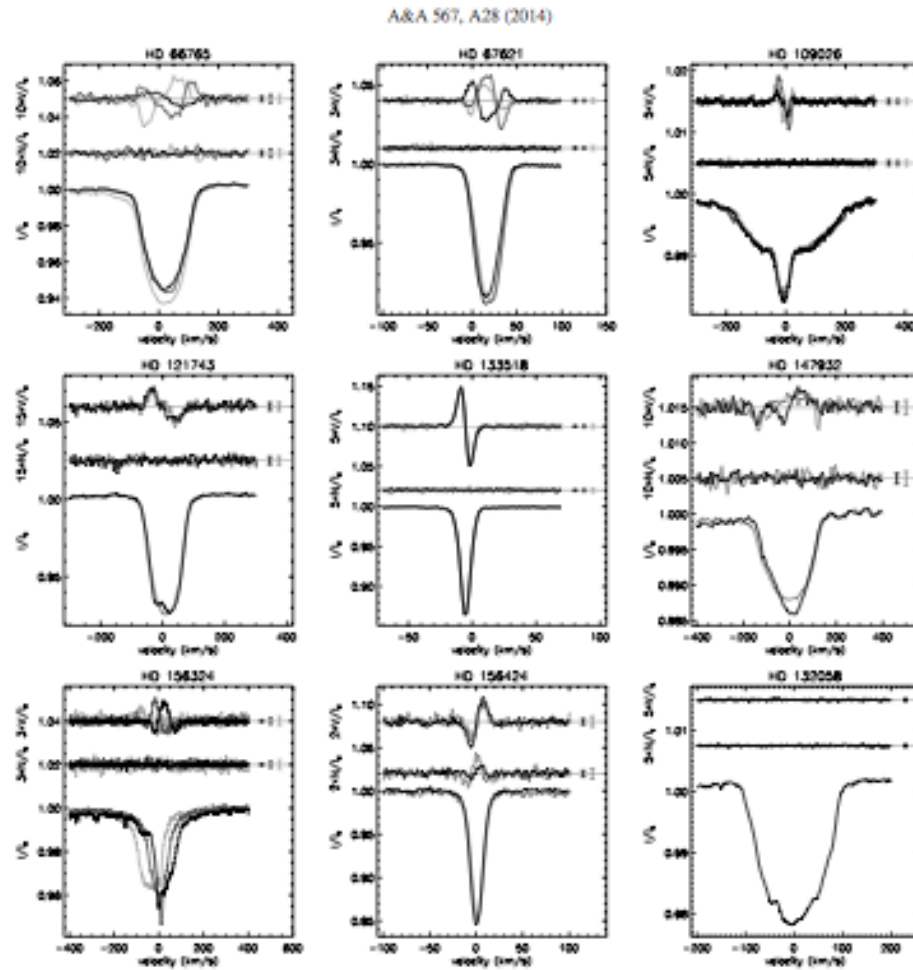
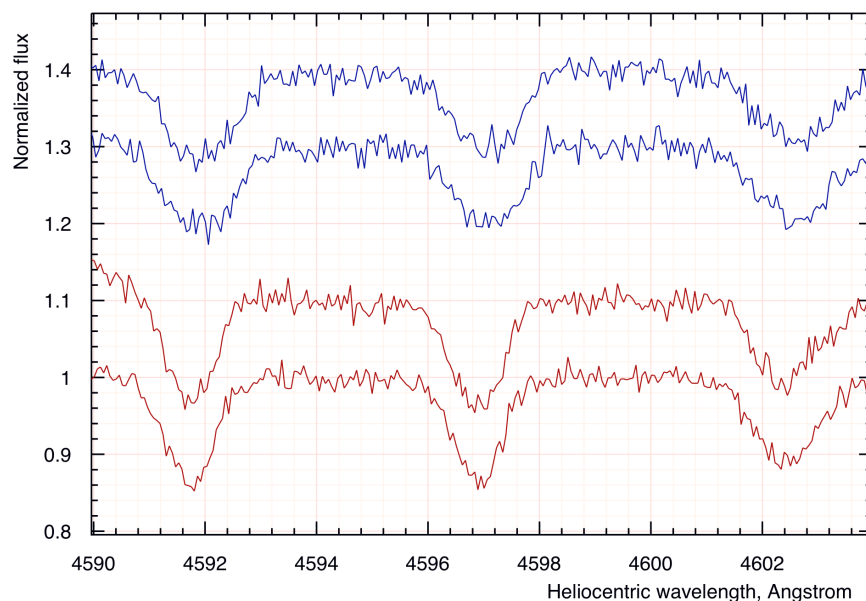


Fig. 2. LSD I (bottom), V (top) and N (middle) profiles of the stars of our sample. For comparison, the profiles of a star with no detected field, HD 132058, are also plotted. The V and N profiles have been shifted and multiplied by a magnification factor for display purpose. The mean error bars in V and N are plotted on the side of each profile. HD 66765: the observations obtained at phases 0.06 (black), 0.43 (light grey) and 0.81 (dark grey) are plotted. HD 67621: the observations obtained at phases 0.11 (dark grey), 0.37 (light grey) and 0.73 (black) are plotted. HD 109026: the observations obtained at phases 0.42 (black), 0.71 (light grey) and 0.95 (dark grey) are plotted. For all other stars, the profiles have been plotted in order of decreasing darkness for decreasing V S/N. The three observations of HD 133518 are almost perfectly superimposed.

Spectral variability in V1449 Aql:

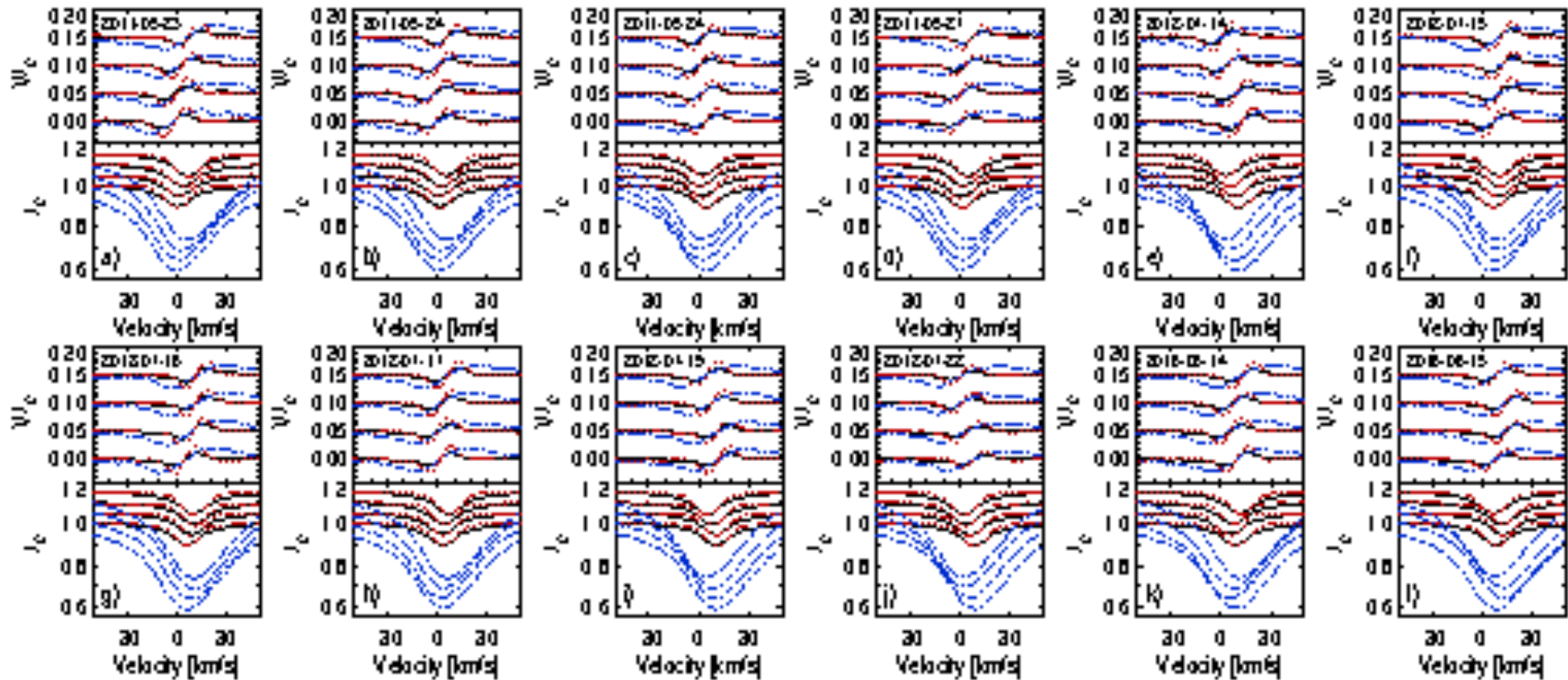
the importance of taking into account pulsations in magnetic field studies



SOFIN $(I \pm V)_0$ and $(I \pm V)_{90}$ spectra taken 20 minutes apart (Hubrig et al. 2011)

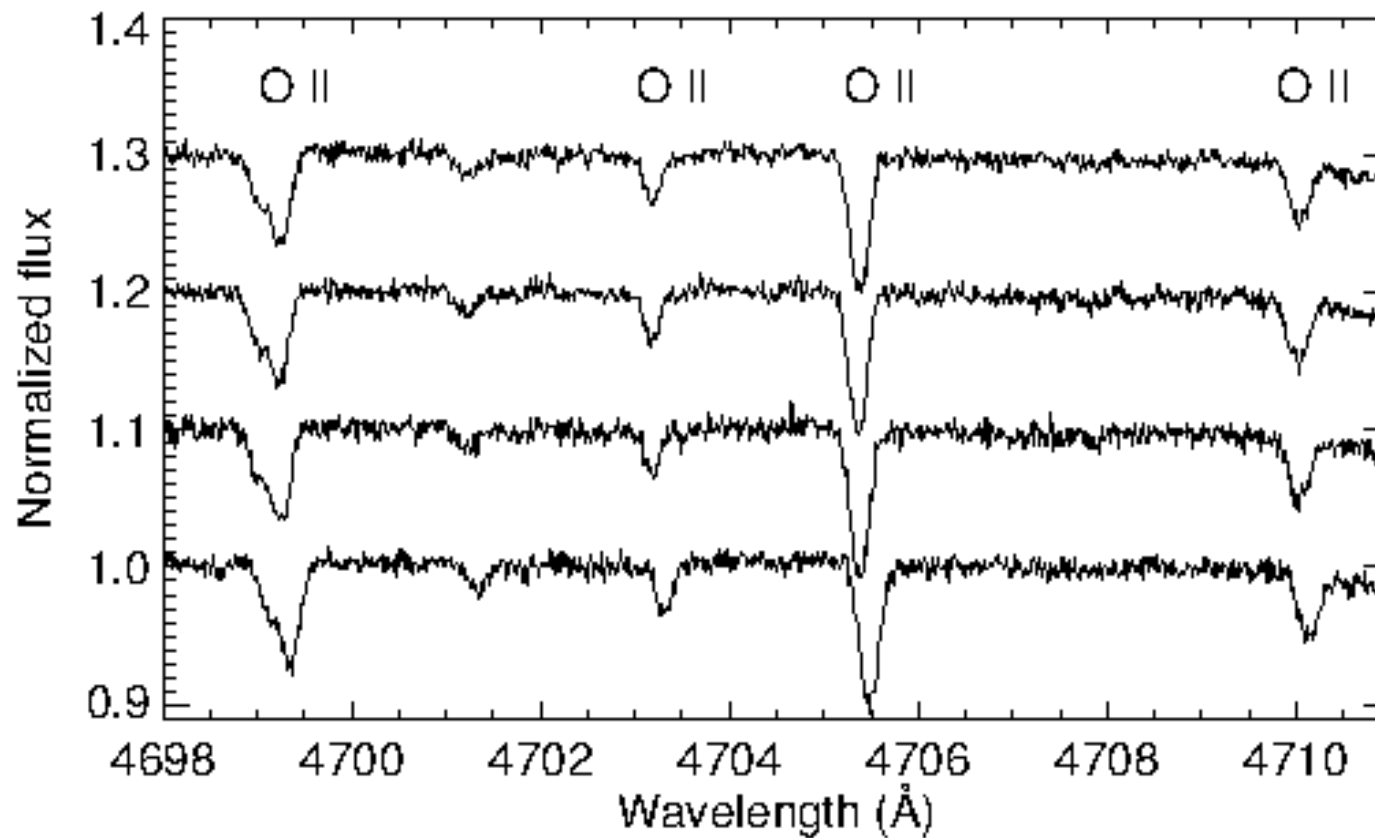
Changes of line shape and position on a 20 minute time scale, different for different elements. Peak-to-peak RV amplitudes reach 90 km/s. $P_{\text{mag/rot}} = 13.89\text{d}$ (13 SOFIN measurements), confirmed by seismic modeling by Aerts et al. (2011).

The case of the strongly magnetic Bp star HD 96446 (Järvinen et al. 2016)



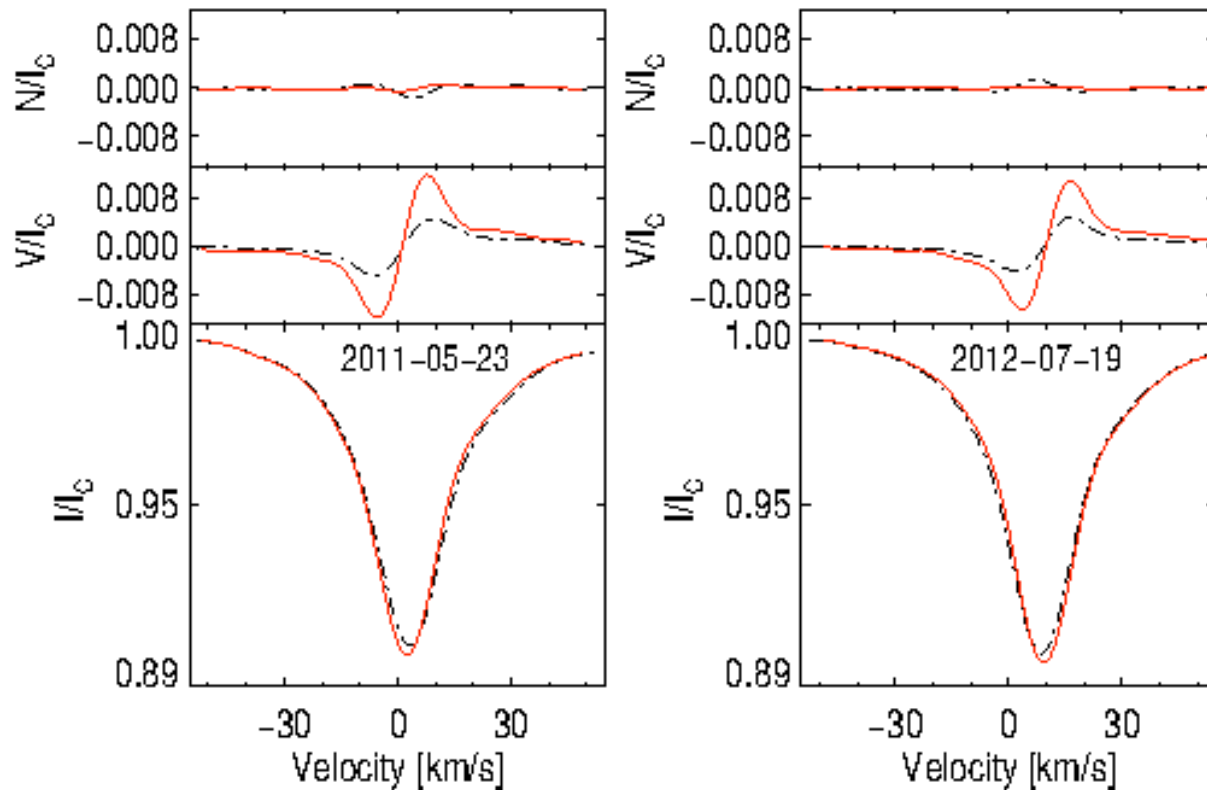
Comparison of Stokes V and I LSD profiles for different line masks.

The case of the strongly magnetic Bp star HD 96446



Changes in line profile shapes between sub-exposures.

The case of the strongly magnetic Bp star HD 96446



$$P_{\text{puls}} = 2.23 \text{ h},$$

$$P_{\text{rot}} = 23.4 \text{ d},$$

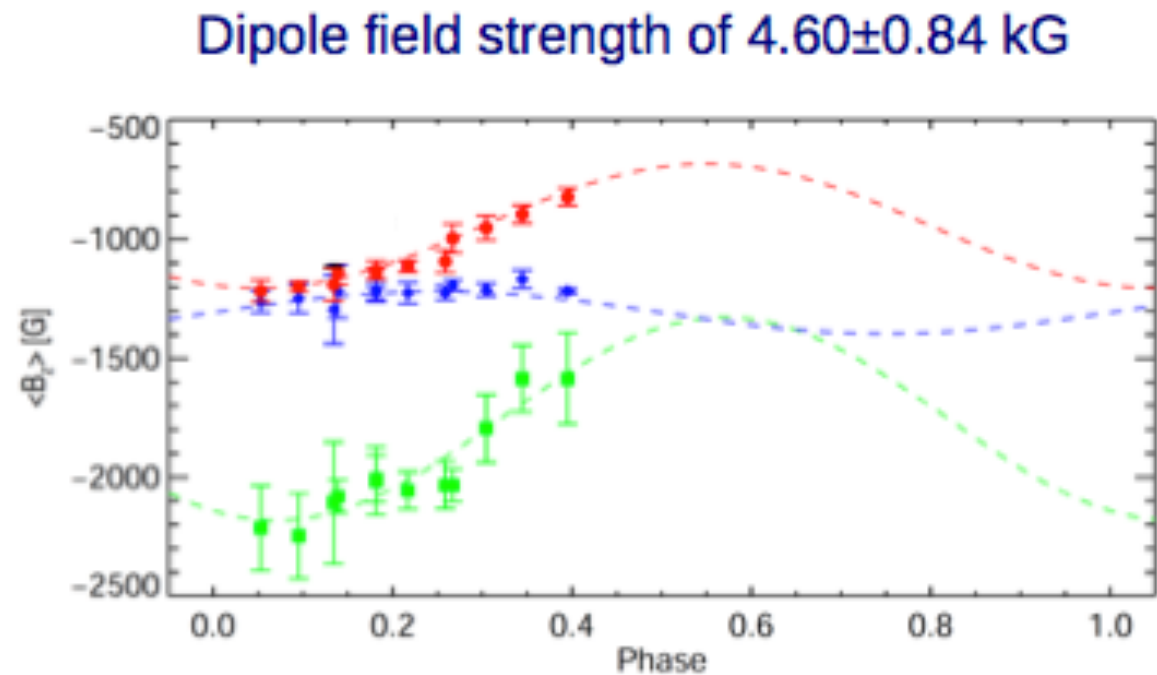
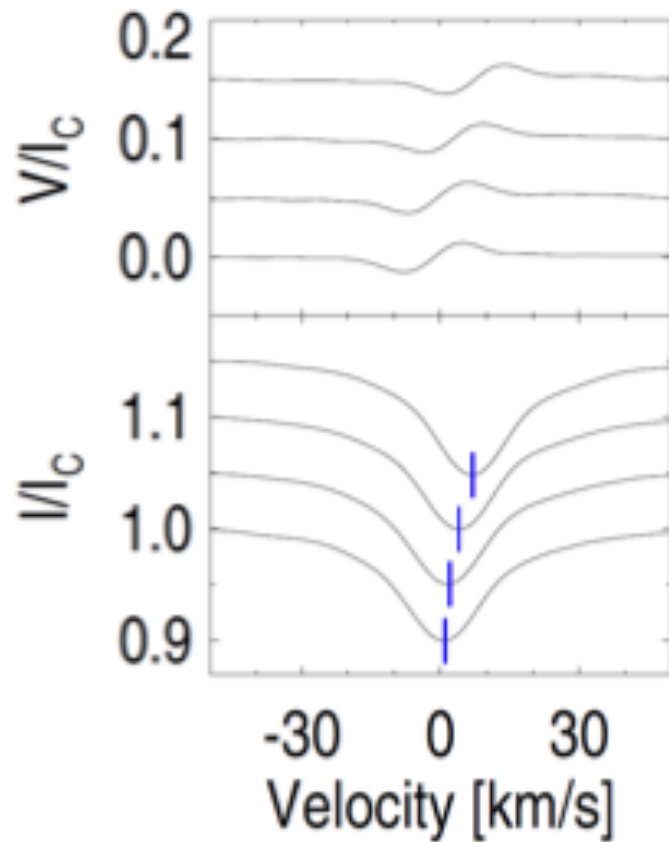
$$P_{\text{orb}} = 808 \text{ d},$$

$$B_d = 4.6 \pm 0.84 \text{ kG}$$

Dashed lines: no correction for the radial velocity shifts.
Solid lines: with correction.

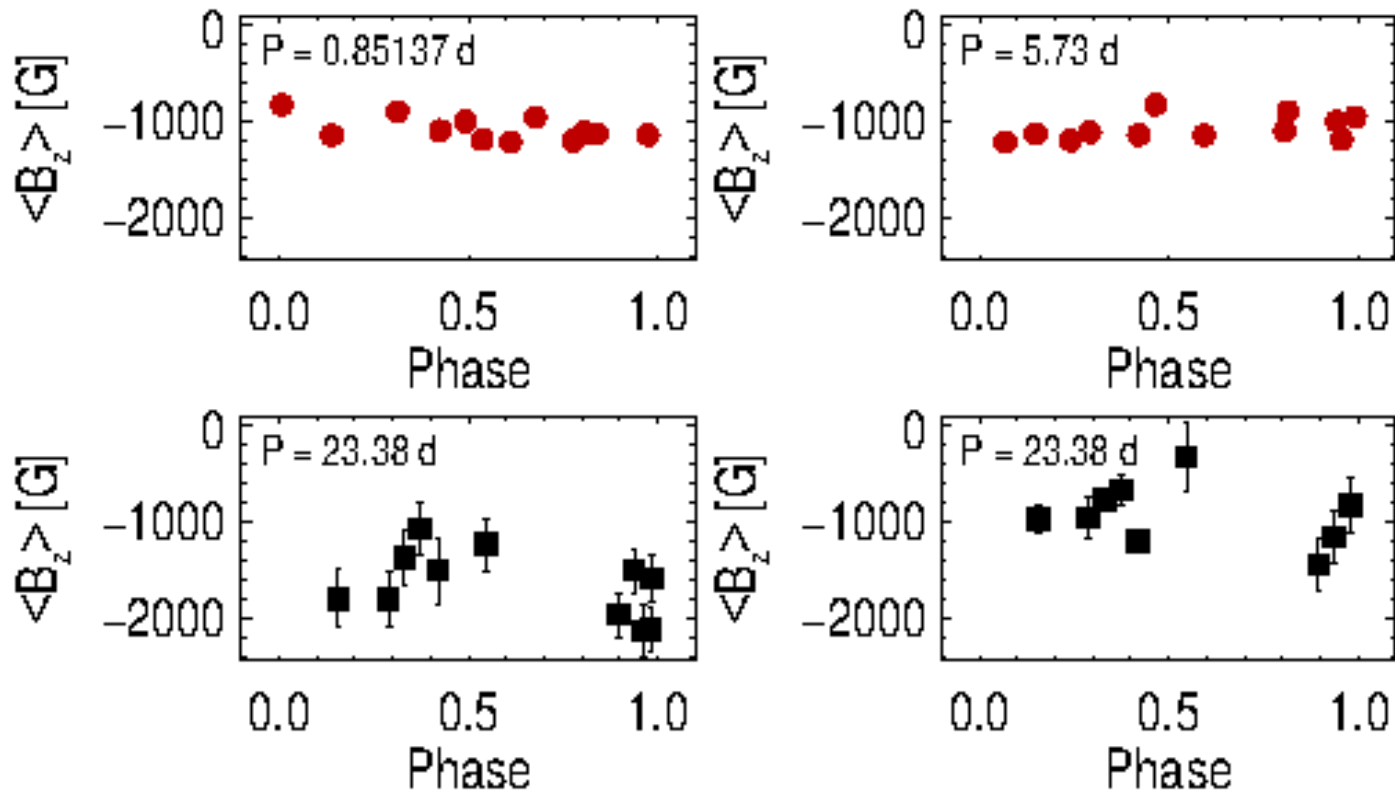
The case of the strongly magnetic Bp star HD 96446

Magnetic field model: a strong dipole strength



Due to stellar pulsation, the line profile varies in each sub-exposure obtained at four different angles, as shown in the left figure (RV shifts and changes in profile shape).

The case of the strongly magnetic Bp star HD 96446



Our magnetic field measurement distribution adopting different rotation periods (upper panel) and the measurement distribution from the literature (low panel).

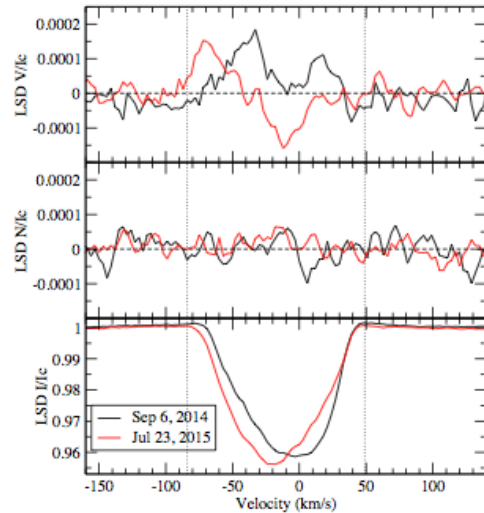


Figure 1. Stokes V (top), N (middle), Stokes I (bottom) LSD profiles of HD 188774 for the first (black) and second (red) measurements. Vertical dotted lines indicate the width of the profile over which the FAP and longitudinal field were calculated.

The exposure time of the sub-exposures corresponds to a significant fraction of the pulsation period (1st observation)

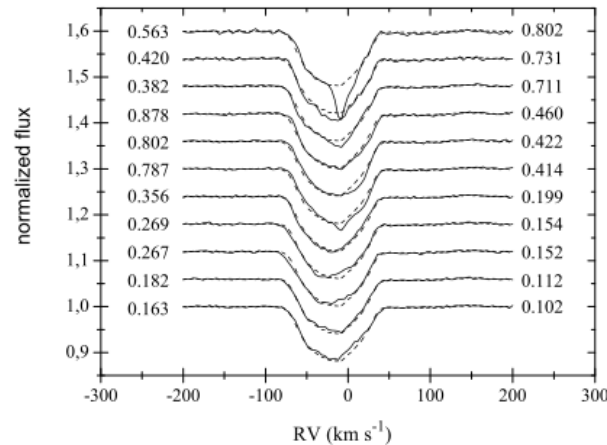


Fig. 4. LSD-profiles computed based on the individual (solid) and mean (dashed) spectra.

No explanation for the features in the LSD profiles, and no chemical spots.

However, Kurtz et al. 2008 was the first to discover $B_z = 47 \pm 13$ G In a δ Scuti star (HD 21190).

Announced as the first δ Scuti star possessing a magnetic field

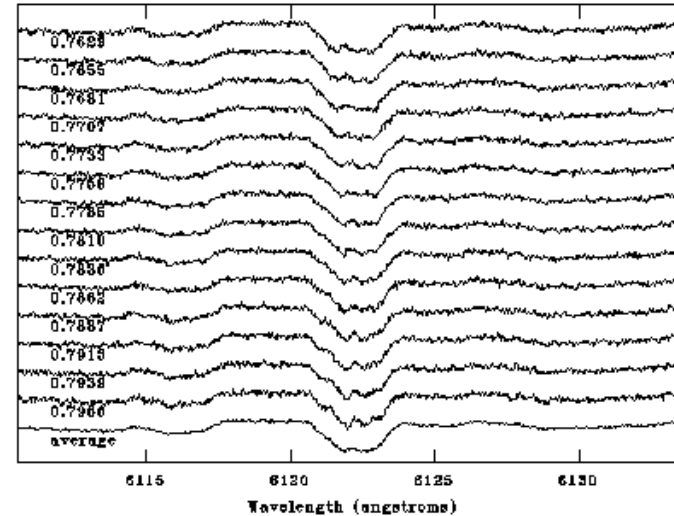
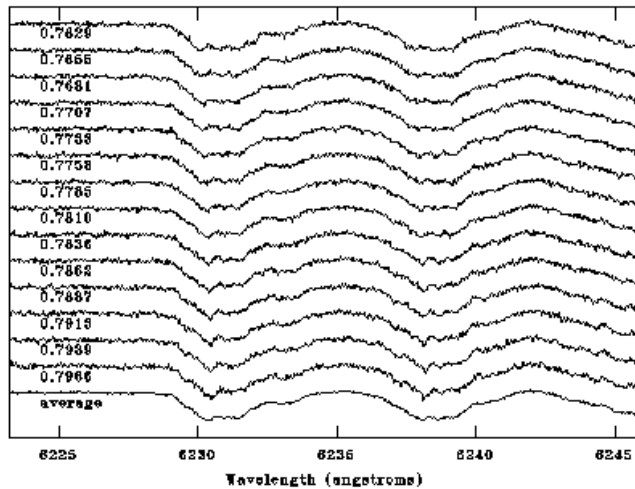
Neiner & Lampens 2015

Discovery of a magnetic field in the δ Scuti star HD 188774 3

Table 1. Spectropolarimetric measurements of HD 188774. The dates, heliocentric Julian dates corresponding to the middle epoch of the measurements, and exposure times are given. The computed longitudinal field B_l and N values, with their respective error bars σ and significance level z are also shown, as well as the field detection probability in % and in terms of type of detection.

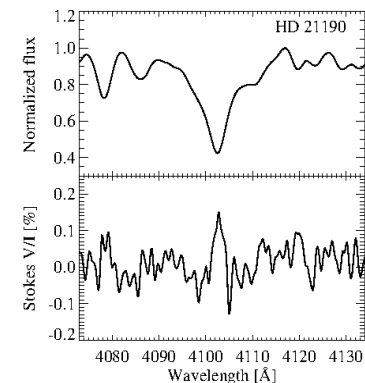
Date	Mid-HJD -2450000	T_{exp} s	$B_l \pm \sigma_B$ G	z_B	$N \pm \sigma_N$ G	z_N	Prob. %	Detect.
Sep 7, 2014	2456907.951	4×840	23.2 ± 17.1	1.4	6.9 ± 17.1	0.4	99.999%	Definite
Jul 23, 2015	2457227.027	10×4×129	75.8 ± 13.0	5.8	7.6 ± 12.9	0.6	100%	Definite

UVES and FORS1 observations of the δ Scuti star HD 21190 (Gonzalez et al. 2008; Kurtz et al. 2008)

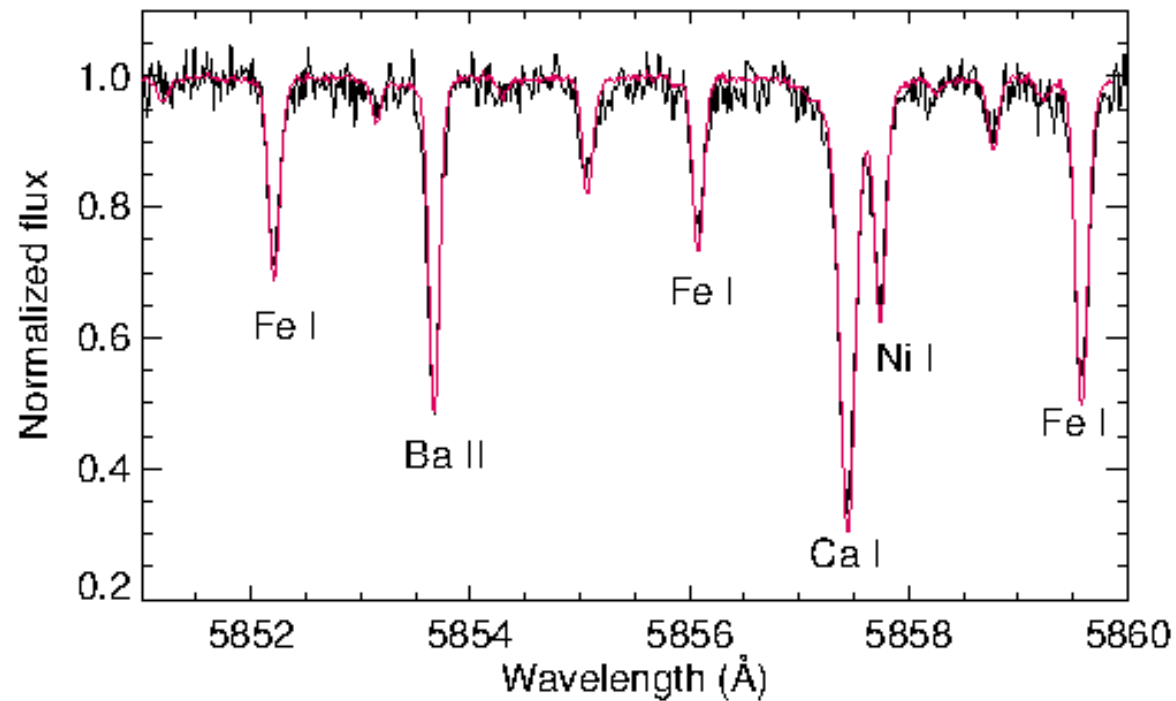


Moving peaks in the cores of spectral lines indicating the presence of high-degree non-radial pulsations (50min \rightarrow 14 UVES spectra).

Stokes I and V/I spectra in the vicinity of the H δ line.



HARPS observations of the companion CPD -83 64B ($V < 10.8^m$ Koen et al. 2001) of the δ Scuti star HD 21190



HARPS secondary spectrum (black) overplotted with the HARPS solar spectrum (red).



Herbig Ae/Be stars

Herbig Ae/Be stars show clear signatures of surrounding disks as evidenced by a strong infrared excess and are actively accreting material. The phase between protostar and main-sequence object is a key stage for planet formation: dusty disks provide the material needed for the formation of planets.



AI

Table 2. rms longitudinal magnetic field strength, rms standard error and reduced χ^2 values of late Herbig Be and Herbig Ae stars. N gives the number of measurements for the individual targets, separately for the low-resolution spectrographs FORS 1 and FORS 2 and the high-resolution spectrographs HARPS, ESPaDOnS and Narval.

Name	Sp. T.	N_{lowres}	N_{hires}	$\overline{\langle B_z \rangle}$ (G)	$\bar{\sigma}$ (G)	χ^2/n	References
PDS 2	F2	3	2	75	25	14.69	W07 H09 H15
HD 31648	A3	2	5	416	125	9.25	H07 W07 H11b A13a
HD 35929	F2	1	5	54	23	5.84	W07 A13a
HD 36112	A5	1	2	89	84	1.11	W07 A13a
V380 Ori	A1	3	24	348	137	10.09	W05 W07 A09
BF Ori	A2	1	2	87	36	16.18	W07 A13a
HD 58647	B9	0	1	218	69	9.98	H13
Z CMa	B9	1	0	1231	164	56.34	S10
HD 97048	A0	19	0	105	58	4.64	W07 H09 H11b
HD 98922	A2	1	2	135	64	6.33	W07 A13a H13
HD 100546	B9	2	0	106	52	7.40	W07 H09
HD 101412	A0	16	0	273	53	33.11	W05 W07 H09 H11a
HD 104237	A4	3	2	56	35	5.75	D97 W07 H13
HD 135344A	A0	2	1	80	85	5.76	H09 A13a
HD 139614	A7	6	3	73	26	8.33	W05 H07 H09 A13a
HD 144432	A7	6	1	100	50	3.52	H07 W07 H09 A13a
HD 144668	A7	2	3	106	34	8.55	H07 W07 H09 A13a
HD 150193	A1	15	1	159	136	6.84	H09 H11b A13a
HD 176386	B9	15	1	130	81	4.28	H09 H11b A13a
HD 190073	A1	6	68	62	21	16.10	C07 H07 W07 H09 A13b H13

References: A09 – Alecian et al. (2009); A13a – Alecian et al. (2013a); A13b – Alecian et al. (2013b); C07 – Catala et al. (2007); D97 – Donati et al. (1997); H07 – Hubrig et al. (2007); H09 – Hubrig et al. (2009); H11a – Hubrig et al. (2011a); H11b – Hubrig et al. (2011b); H13 – Hubrig et al. (2013); H15 – this Letter; S10 – Szeifert et al. (2010); W05 – Wade et al. (2005); W07 – Wade et al. (2007).

Hubrig et al. 2015



Density distribution of the rms $\langle B_z \rangle$ values for Herbig Ae/Be stars with measured fields: only very few stars have fields stronger than 200 G and half of the sample possesses fields of about 100 G and less. Previous measurements (ESPaDOnS + Narval – Alecian et al. 2013) show measurement uncertainties worse than 200 G for 35% and 100-200 G for 32% of the measurements.

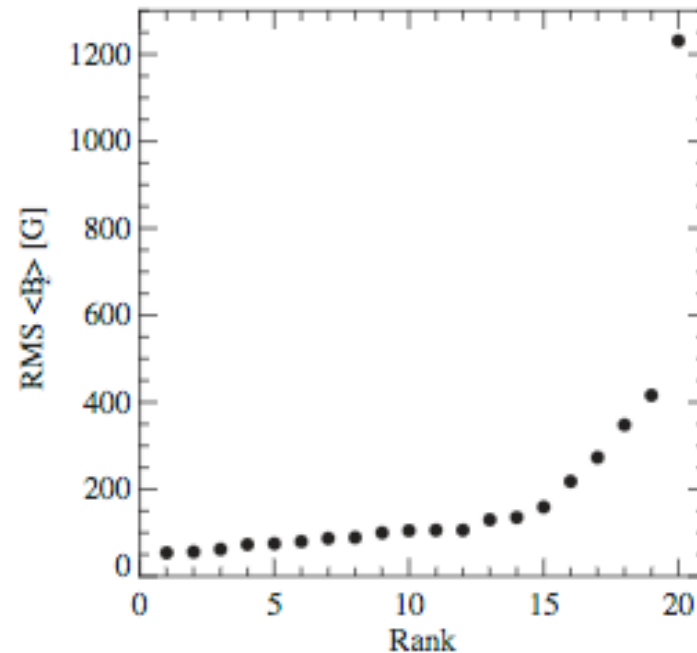


Figure 3. Density distribution of the rms longitudinal magnetic field values (Col. 4 in Table 2) for the twenty late Herbig Be and Herbig Ae stars for which detections of a magnetic field were reported in the past.

HARPS polarimetry of sharp-lined Herbig Ae stars

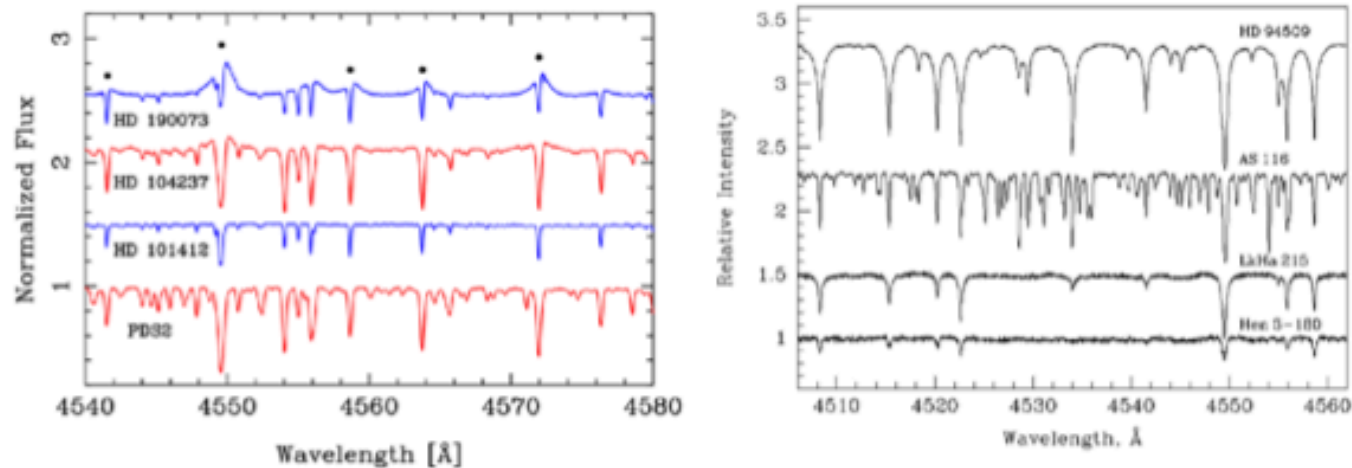


Fig. 1. *Left:* High-resolution HARPS spectra in integral light of the weakly magnetic ($B_d \approx 0.3$ kG) Herbig Ae stars HD 104237, PDS 2, and HD 190073, and the strongly magnetic ($B_d \approx 3$ kG) Herbig Ae star HD 101412. Filled circles mark metallic lines appearing sometimes in emission. *Right:* UVES spectra of a few Herbig Ae/Be stars with low $v \sin i$ values.



The non-pulsating Herbig Ae star PDS 2 ($\langle B_z \rangle = 103 \pm 29$ G in FORS1 observations)

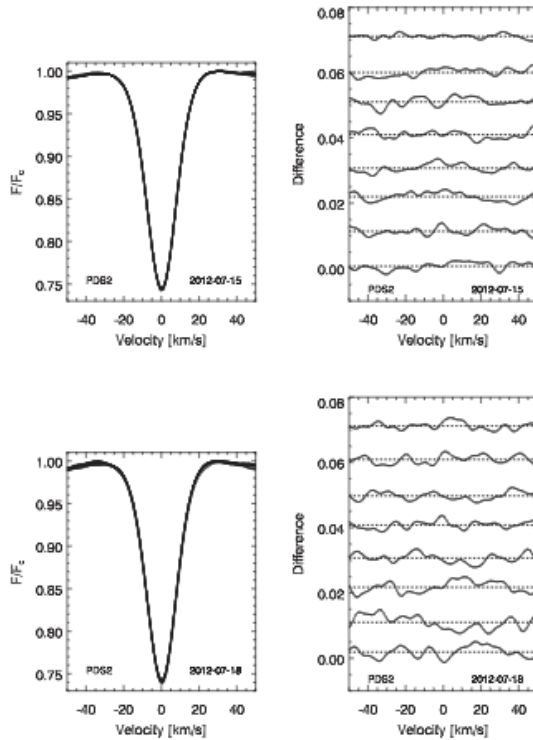


Figure 1. Comparison of the SVD Stokes I profiles in the subexposures recorded on the nights of 2012 July 15 (top) and 18 (bottom). Left-hand panels: overplotted Stokes I profiles computed for the individual subexposures obtained with a time lapse of 15 min. Right-hand panels: differences between the Stokes I profiles computed for the individual subexposures and the average Stokes I profile.

$\langle B_z \rangle = 33 \pm 5$ G on the second epoch
 (Hubrig et al. 2015)

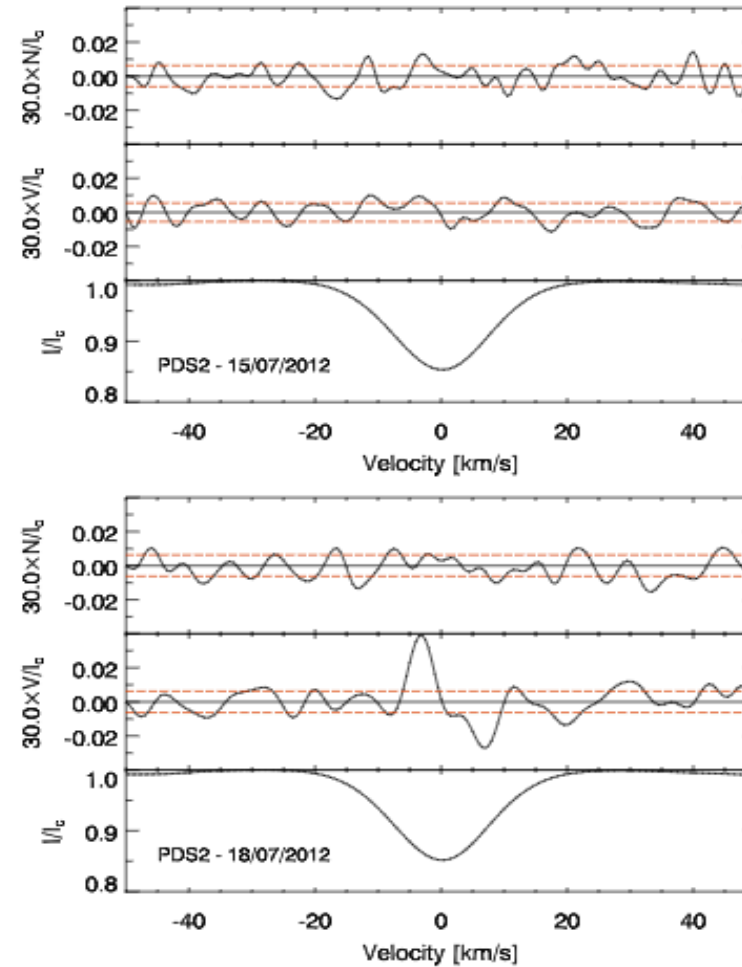


Figure 2. I , V and N SVD profiles obtained for PDS 2 on two different nights. The V and N profiles were expanded by a factor of 30 and shifted upwards for better visibility. The red dashed lines indicate the standard deviations for the V and N spectra.

Magnetic field in the components of the SB2 system HD 104237

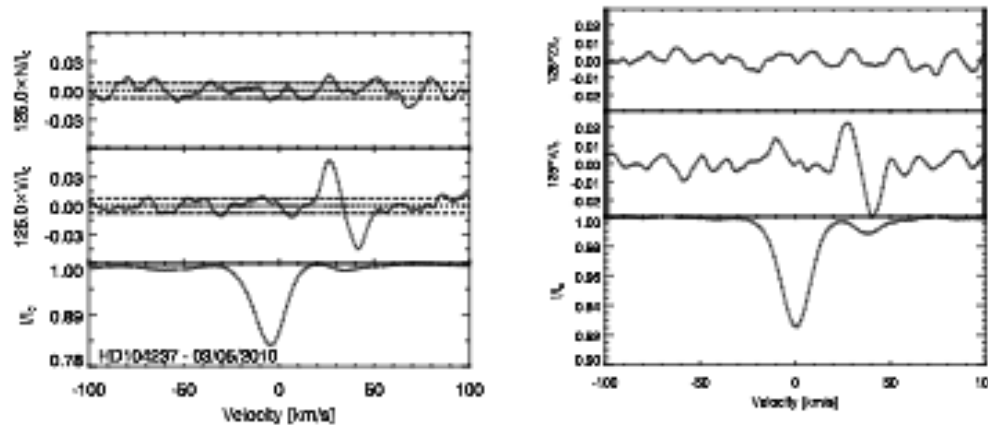


Fig. 5. The SVD I , V , and N spectra of HD 104237 obtained with different samples of metallic lines. The dashed lines in the plot on the left side indicate the standard deviations for the N and V spectra.

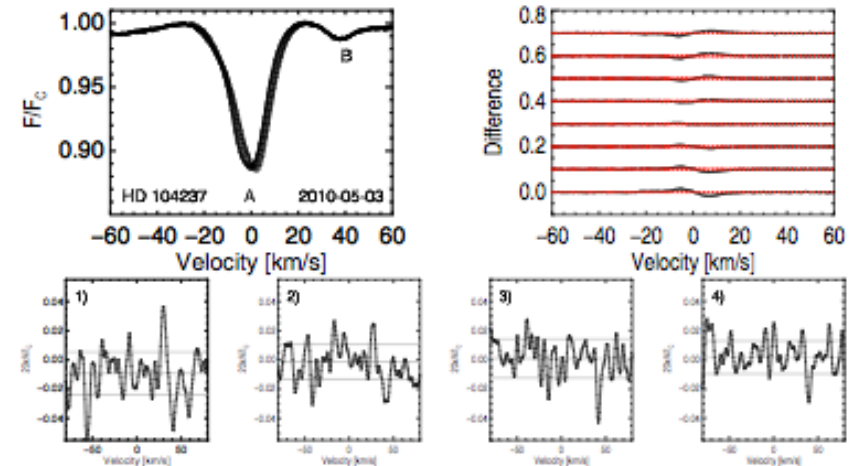


Fig. A.2. Upper row: comparison of the LSD Stokes I profiles of HD 104237 computed for the individual subexposures obtained with a time lapse of 2.2 min (left side) and differences between Stokes I profiles computed for the individual subexposures and the average Stokes I profile with standard deviation limits indicated by the dashed lines (right side). Lower row: Stokes V spectra calculated for the combination of pairs of two subexposures with the quarter-wave plate angles separated by 90 degrees, four pairs in all.

$\langle B_z \rangle = 129 \pm 12$ G in the T Tauri component, but only about 13 G in the primary.

The primary is a δ Scuti-like pulsator.

(Järvinen et al. 2015)

Variable magnetic field in the Herbig Ae star HD 190073

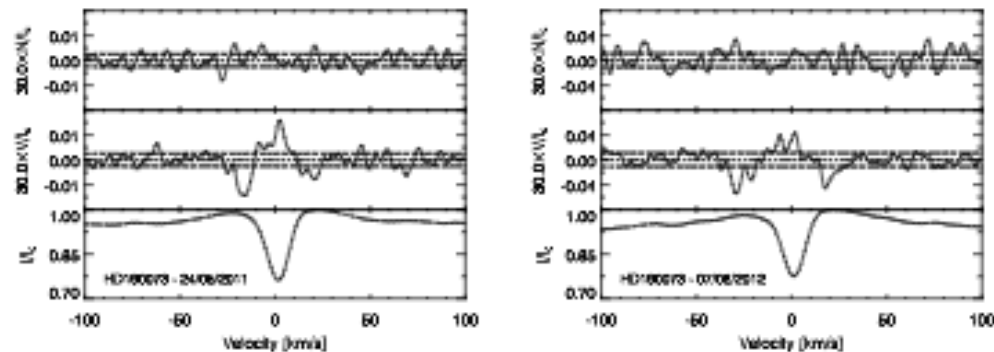


Fig. 6. SVD I , V , and N spectra of HD 190073 obtained using a sample of 287 metallic lines at the first epoch and 522 metallic lines at the second epoch. The dashed lines indicate the standard deviations for the N and V spectra.

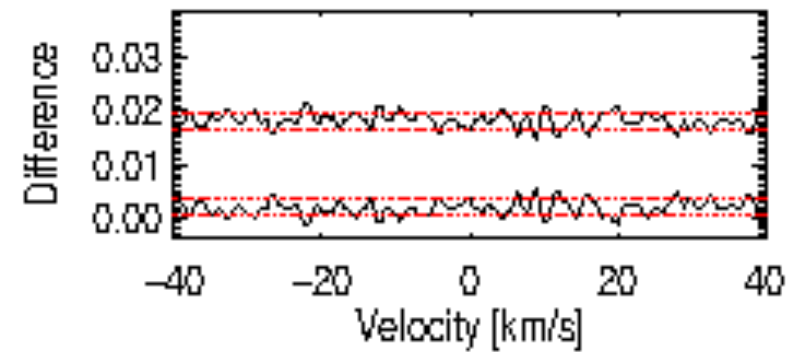
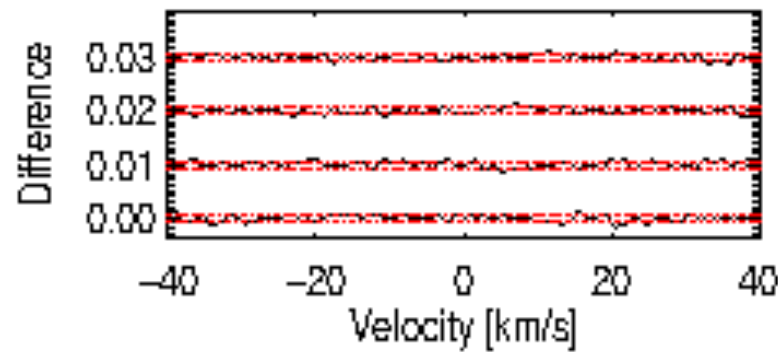
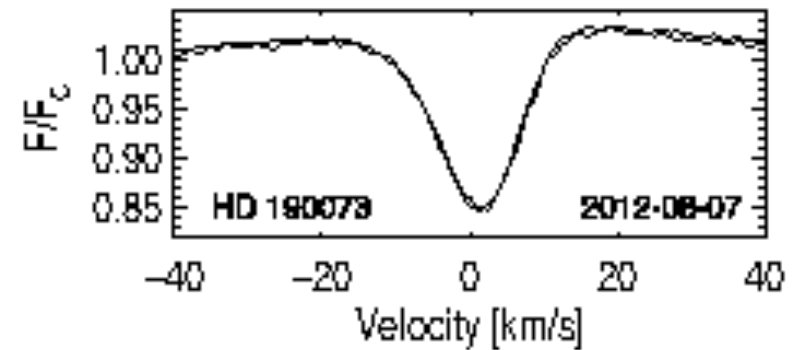
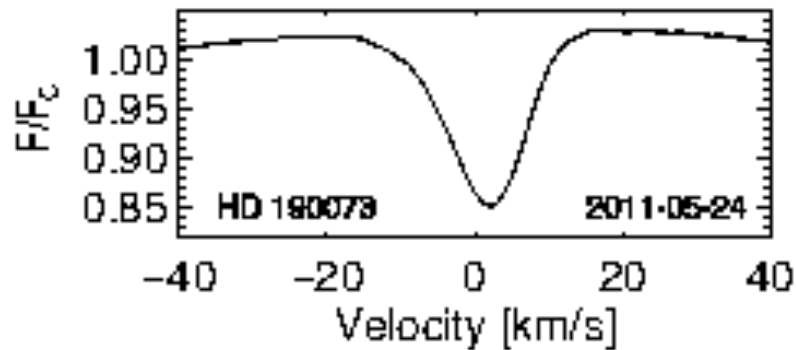
$$\langle B_z \rangle = -8 \pm 6 \text{ G (in 2011)}$$

$$\langle B_z \rangle = -15 \pm 10 \text{ G (in 2012)}$$

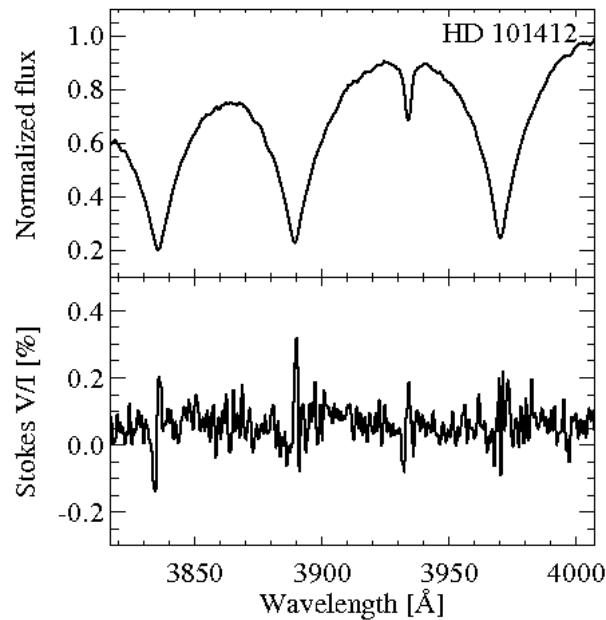
Hubrig et al. 2006: $84 \pm 30 \text{ G}$

Catala et al. 2007: $74 \pm 10 \text{ G}$

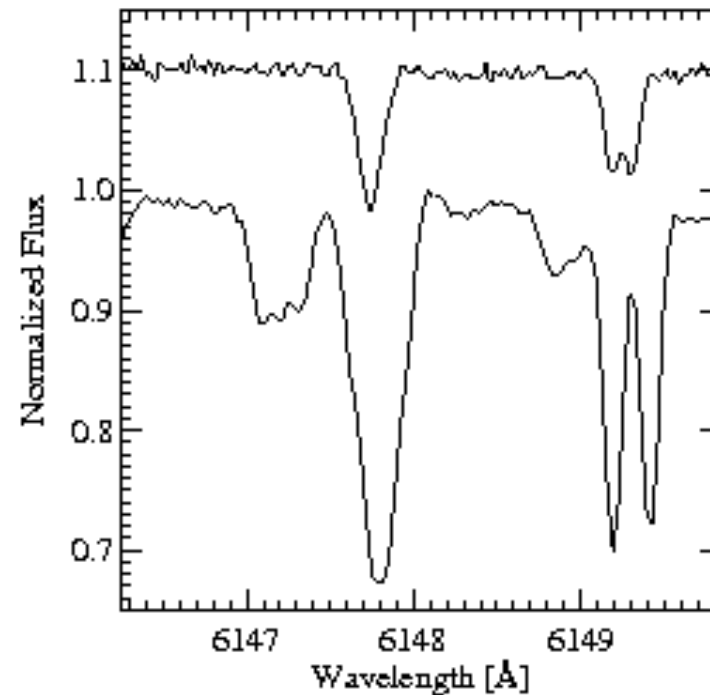
Variable magnetic field in the non-pulsating Herbig Ae star HD 190073



The currently best-studied, sharp-lined Herbig Ae star HD 101412 with a strong surface magnetic field

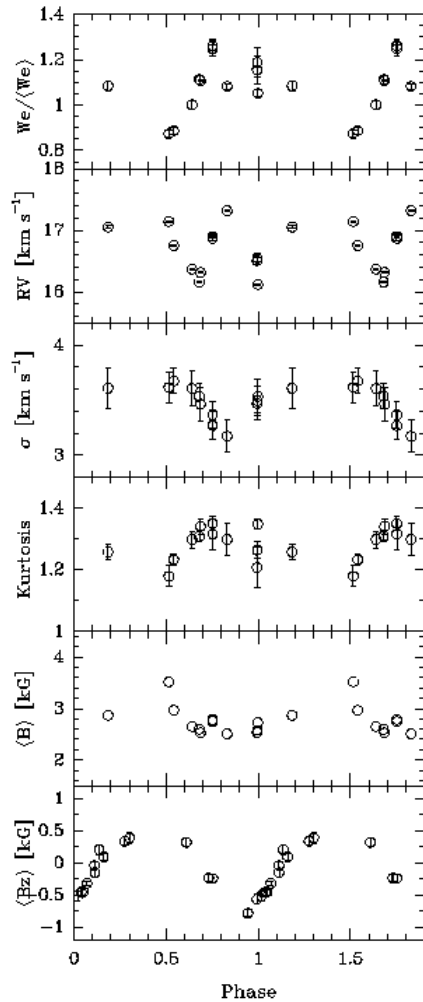


Zeeman features in H9, H8,
Ca II H&K, and He profiles
(Hubrig et al. 2011)

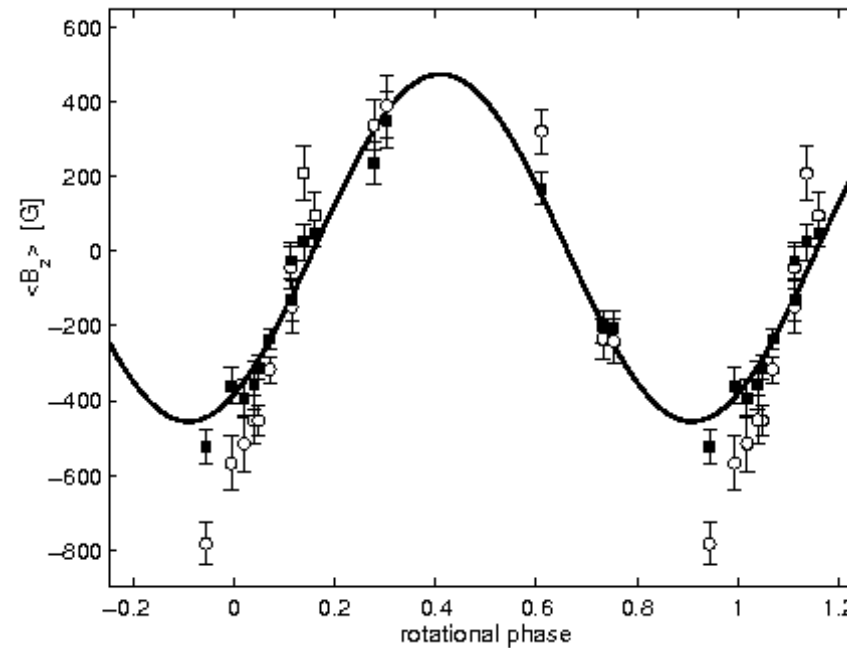


Stokes *I* spectra of the Herbig Ae star HD 101412 ($\langle B \rangle = 2.5$ to 3.5 kG) and the typical Ap star HD 116458 ($\langle B \rangle = 4.7$ kG). The magnetic field modulus is measured using the magnetically split Fe II 6149.258 line.

The magnetic field of the Herbig Ae star HD 101412

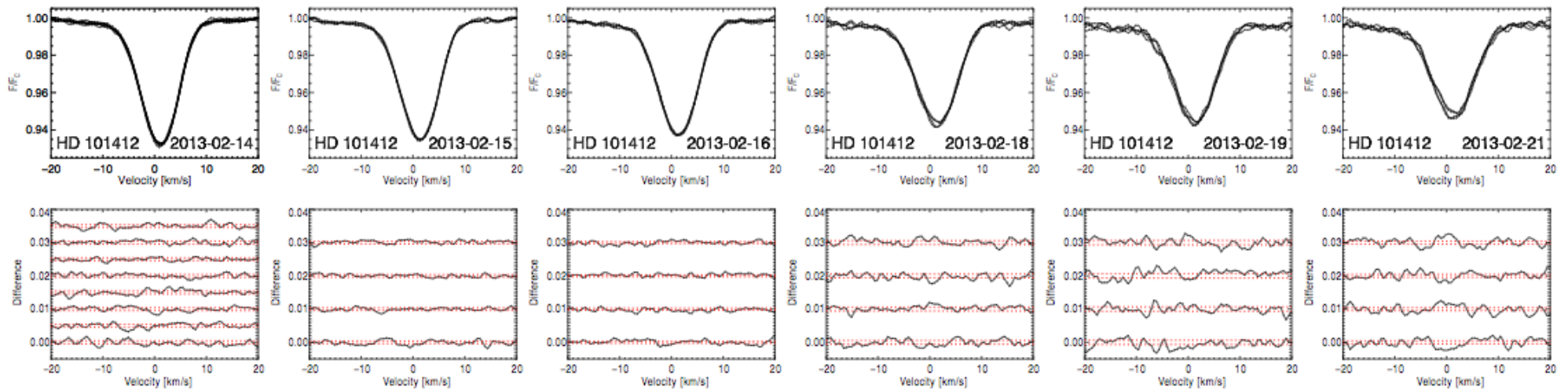


Variability of various observables over the period.



Phase diagram with the best sinusoidal fit for the $\langle B_z \rangle$ measurements using all lines (filled squares) and hydrogen lines (open circles). For $i = 80^\circ$ we calculate a magnetic obliquity $\beta = 84 \pm 13^\circ$. In the magnetospheric accretion scenario the topology of the channeled accretion critically depends on the magnetic obliquity: For such a large dipole inclination, many field lines would thread the inner region of the disk matter, causing strong magnetic braking (Romanova et al. 2003).

Magnetic field of the Herbig Ae star HD 101412



Comparison of the LSD Stokes I profiles computed for individual sub-exposures and the differences between individual profiles and the average Stokes I profile



Take-away messages

- Several massive pulsating stars possess large-scale organised magnetic fields of the order of kG down to a few Gauss. Special care has to be taken in the magnetic field analysis due to the presence of significant changes in the line profile position and profile shape over the whole observational cycle at 4 positions of the retarder waveplate.
- Spectroscopic/spectropolarimetric observations can be successfully used for the detection of δ Scuti-like pulsations in pre-main sequence stars in analogy with previous UVES time series observations of roAp stars.